ACS APPLIED MATERIALS & INTERFACES

Research Article

www.acsami.org

Recycling Rare Earth Elements from Industrial Wastewater with Flowerlike Nano-$Mg(OH)_2$

Chaoran Li,[†,‡] Zanyong Zhuang,[†,‡] Feng Huang,[§] Zhicheng Wu,[†,‡] Yangping Hong,[†,‡] and Zhang Lin*[,†,‡]

[†]State Key Laboratory of Structural Chemistry, Fujian Institute of Research on the Structure of Matter, Chinese Academy of Sciences, Fuzhou, Fujian, 350002 P. R. China

[‡]Key Laboratory of design and assembly of functional nanostructures, Chinese Academy of Sciences, Fuzhou, Fujian, 350002 China

[§]Key Laboratory of Optoelectronic Materials Chemistry and Physical Chemistry, Fujian Institute of Research on the Structure of Matter, Chinese Academy of Sciences, Fuzhou, Fujian, 350002 China

ABSTRACT: Treatment of wastewater containing low-concentration yet highly-expensive rare earth elements (REEs) is one of the vital issues in the REEs separation and refining industry. In this work, the interaction and related mechanism between self-supported flowerlike nano-$Mg(OH)_2$ and low-concentration REEs wastewater were investigated. More than 99% REEs were successfully taken up by nano-$Mg(OH)_2$. Further analysis revealed that the REEs could be collected on the surface of $Mg(OH)_2$ as metal hydroxide nanoparticles (<5 nm). An ion-exchange model was proposed as a critical factor for both guaranteeing the reaction speed and maintaining the self-supported structure of the materials. In addition, a method was developed to further separate the immobilized REEs and the residual magnesium hydroxide by varying the solution pH. In a pilot-scale experiment, the REEs from practical wastewater were immobilized effectively at a high flow rate. We anticipate this work can provide a good example for the recycling of valuable REEs in practical industrial applications.

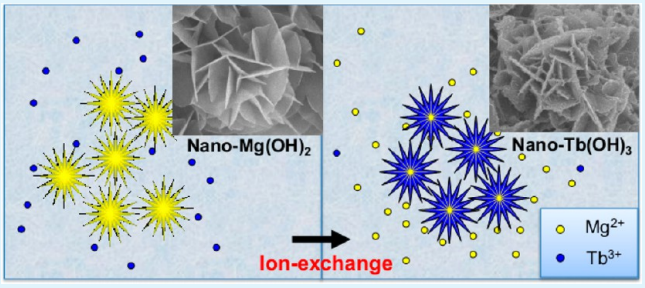

KEYWORDS: *$Mg(OH)_2$ nanoparticles, rare earth elements, recycling, self-supported, ion-exchange, water treatment*

1. INTRODUCTION

Due to the special metallurgical, optical, and electronic properties, rare earth elements (REEs) play irreplaceable roles in designing magnetic,[1] luminescent,[2] catalytic,[3] hydrogen storage,[4] and superconductive materials.[5] Nevertheless, the small global reserve of REEs of no more than 99 million tons limits their use.[6] For instance, it is reported that the mining of Tb and Dy can only last 30 years. Hence, the recycling of REEs is an urgent task.

While a number of studies deal with recycling REEs from post-consumer rare earth products,[7−10] others aim at developing various recovery methods, e.g., liquid membrane,[11] precipitation,[12,13] and sorption[14] from the REEs water of high concentrations. However, the REE concentrations in most wastewater are as low as one to hundreds of mg/L despite the high total annual wastewater generation of more than 7.2 million tons. Traditional adsorbents, e.g., zeolite, clay, and active carbon,[15] show high adsorption capacity under the condition of high metal ion concentrations, but they are usually not suitable for dilute metal ion solutions because of their weak extraction force. In the unrecoverable event with available adsorbents, the REEs are disposed into the environment as industrial wastewater.

Over the past few decades, the use of nanomaterials in the water treatment field has attracted broad interests. Compared to traditional bulk material, nanomaterials exhibit larger specific surface area, higher surface activity, and more active sites. Hence, nanomaterials often exhibit high efficiency in extracting metal ions of low concentrations.[16−20] Moreover, the morphology and structure of nanomaterials are tunable to meet the needs of practical applications. From the material selection perspective, most studies tend to pay more attention to the properties of the nanomaterials but ignore their practical aspects including cost-effectiveness, toxicity, extraction efficiency, structure versatility, and stripping/enrichment. To date, existing studies only address part of the issues raised above; hence, there are few practical commercial products.

Nano-$Mg(OH)_2$, an environmentally friendly material, exhibits a large specific surface area, high activity, and extraction ability. Previously, it has been proven to show good ability in removing heavy metals or dye molecules from the wastewater.[21−24] Our group has also made great efforts to treat environmentally diluted wastewater with nano-$Mg(OH)_2$ for the pre-enrichment of low-concentration heavy metals such as chromium and uranium.[16,21] However, the process and mechanisms of REEs recycling by $Mg(OH)_2$ remain poorly understood.

Theoretically, the following reaction may take place.

Received: July 13, 2013
Accepted: September 13, 2013
Published: September 13, 2013

   dx.doi.org/10.1021/am4027967 | ACS Appl. Mater. Interfaces 2013, 5, 9719−9725

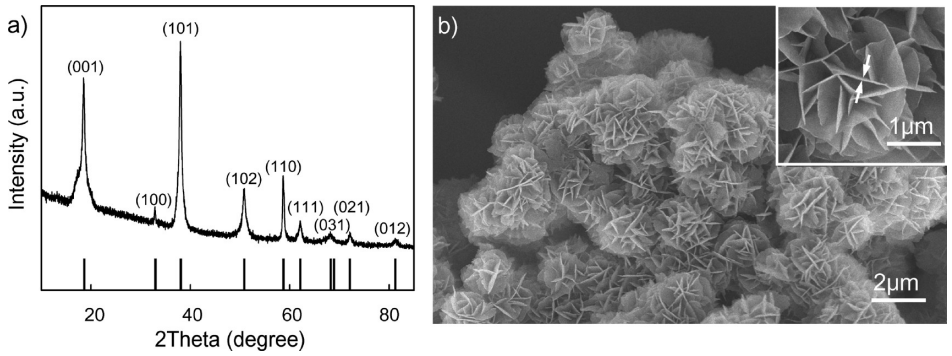

Figure 1. Typical (a) XRD pattern and (b) SEM image of follower-like nano-$Mg(OH)_2$ prepared by the hydration of magnesium sulfate. The inset of (b) is an enlarged SEM image showing a single flowerlike magnesium hydrate.

$$3Mg(OH)_2 + 2RE^{3+} \rightarrow 2RE(OH)_3 + 3Mg^{2+} \quad (1)$$

The equilibrium constant k, expressed as $K_{spMg(OH)2}{}^3/K_{spRE(OH)3}{}^2$, has a large value of 1.5×10^5 to 9.1×10^{27}. The k values for scarce heavy REEs are generally higher than those of light ones. The large k values suggest that $Mg(OH)_2$ should be able to extract REEs from their dilute solutions potentially at high efficiencies. Moreover, the morphology of nano-$Mg(OH)_2$ can be kinetically controlled. The self-supported structure of nanomaterial is very promising in practical applications for the following reasons. First, this structure ensures adequate contact with the pollutants. Second, self-supported nanomaterials are kinetically favored to maintain the flow velocity in the extraction process while avoiding aggregation and clogging problems that nanomaterials frequently encounter.[25,26]

In this work, a strategy was devised for the recovery of REEs from wastewater at the REE concentrations of dozens to hundreds of mg/L during the rare earth separation and purification process. Self-supported flowerlike nano-$Mg(OH)_2$ was synthesized and characterized. The mechanism and efficiency between $Mg(OH)_2$ and some valuable REEs (Eu, Tb, Dy, Yb) were evaluated. It is our goal to achieve efficient extraction, enrichment, and recovery of low concentrations of REEs.

2. EXPERIMENTAL SECTION

Material. All chemicals were of reagent grade. All solutions were prepared using deionized water. Ammonium hydroxide (NH_4OH, AR) and magnesium sulfate ($MgSO_4$) were obtained from National Medicines Co., Ltd. of China. Lanthanide chlorides were purchased from Aladdin Reagent (Shanghai) Co., Ltd. The commercial $Mg(OH)_2$ was purchased from Tianjin Fuchen Chemical Reagent Factory, China. The columns were obtained from Synthware Glass.

Preparation of Nano-$Mg(OH)_2$. Nano-$Mg(OH)_2$ was prepared by the precipitation method at a controlled temperature of 60 °C. Ammonia was added dropwise to 2 mol/L $MgSO_4$ solution at a stirring speed of 3000 r/min. Stirring was ceased when the pH of the solution reached 10.5. After aging for 2 h, the suspension was centrifuged at 8000 rpm for 2 min and washed with distilled water for three times. The precipitate was collected and dried for the XRD analysis, SEM study, and BET measurement.

Uptake of Tb^{3+} by Nano-$Mg(OH)_2$. A Tb^{3+} solution was prepared by dissolving 0.2 mmol of $TbCl_3{\cdot}6H_2O$ in 50 mL of deionized water. To this solution was added 0.3 mmol $Mg(OH)_2$, prepared in the previous step under continuous stirring. At different time intervals, 1 mL of the solution was taken out, centrifuged, and briefly rinsed twice with alcohol. The precipitates were then dried in the oven at 60 °C for 2 h. The solid product was thus obtained and ready for the XRD and ICP-AES analyses.

Extraction of Other REEs. Chloride salts (0.2 mmol) of cerium, europium, terbium, dysprosium, and ytterbium were dissolved in 50 mL of deionized water, respectively. Nano-$Mg(OH)_2$ powder (0.3 mmol) was added to each solution. After continuous stirring for 1 h, the suspension was centrifuged. The precipitate was washed with distilled water and ethanol and then dried at 60 °C for 2 h. The solid powder was characterized by XRD.

Column Extraction. One gram of self-supported flowerlike nanomagnesium hydroxide prepared in the first step was transferred into a glass column with a diameter of 3 cm. Then, the column was flushed with 10.2, 94.3, and 946 mg/L Tb^{3+} solution at the rate of 5 mL/min, respectively. N_2 was infused at the top of the sealed column to adjust the pressure and control the flow rate. Tb^{3+} concentration was analyzed by ICP-AES before and after the flush.

Pilot-Scale Experiment. Practical industrial wastewater containing REEs was used for the pilot scale experiment. The REEs concentration of the solution was 127.42 mg/L with pH adjusted to 7.0. Wastewater (30 L) passed through the column (d = 8 cm, L = 61 cm) filled with 10.0 g of commercial $Mg(OH)_2$ and flowerlike nano-$Mg(OH)_2$, respectively. During the process, a series of the flow velocity and the extraction ratio was measured within 60 min.

To further purify REEs, the solid in the column was transferred to a small amount of aqueous solution. After adjusting the pH to 7 with 1.0 M HCl, the residual $Mg(OH)_2$ was dissolved. After calcination, pure rare earth oxides were obtained.

Characterization. The phases of the samples were identified by the XRD patterns obtained on a PANalytical X'Pert PRO diffractometer with Cu KR radiation (40 kV, 40 mA) in the continuous scanning mode. The 2θ scanning range was from 5 to 75 in steps of 0.017 with a collection time of 20 s per step. The average crystallite size was calculated from the peak broadening using the Scherrer equation. The morphology and size of the solid product were characterized on a JSM-6700F scanning electron microscope equipped with an Oxford-INCA energy dispersive X-ray (EDS) spectrometer and a JEOL JEM2010 transmission electron microscope (TEM) at 200 KV. The content of Mg and Tb in the solid product was determined by inductively coupled plasma atomic emission spectrometry (ICP-AES, Jobin Yvon Ultima2). Specific surface area of the sample was measured with an accelerated surface area and porosimetry analyzer (Micromeritics' ASAP 2020).

3. RESULTS AND DISCUSSION

Characterizations of Nano-$Mg(OH)_2$. Figure 1 shows the typical XRD pattern and SEM images of the nano-$Mg(OH)_2$ prepared by the chemical precipitation method. As shown in Figure 1a, the XRD pattern reveals that diffraction peaks can be well-indexed as hexagonal magnesium hydroxide, with a calculated crystallite size of 16.9±0.8 nm in the [001] direction and 22.1±1.1 nm in the [101] direction using the Scherrer equation. Figure 1b shows the typical SEM image of the as-prepared $Mg(OH)_2$. The as-prepared sample was composed of

very uniform flowerlike architecture with approximately 1.8–2.4 μm diameter. Each flowerlike nanostructure was composed of a number of nanoplatelets with a thickness of 10 nm or more, making a spherical self-supported structure. The BET measurement shows that the specific surface area of the nano-$Mg(OH)_2$ is 66.9 m^2/g.

Uptake of Tb^{3+} by Nano-$Mg(OH)_2$. In the Tb^{3+} uptake experiment, the molar ratio of $Mg(OH)_2$ and Tb^{3+} was set at 3:2 based on reaction 1. $Mg(OH)_2$ (3 mmol) was put into a 50 mL Tb^{3+} solution with an initial concentration of 0.04 mol/L. Table 1 shows the contents of Mg and Tb in both the solid and the liquid as a function of time. In the first 30 min, 95.7% Tb^{3+} in the solution can be extracted by $Mg(OH)_2$ as shown by the concentration decrease from 40 to 1.7 mmol/L. The change of the Tb and Mg content in the solid phase was also analyzed. Interestingly, as the percentage of Tb in the solid phase increases from 0% to 54.38%, the content of Mg decreases rapidly from 41.38% to 3.62%, suggesting that magnesium was transferred into the solution as ions. Even if the nano-$Mg(OH)_2$ is not in excess, 95.7% Tb^{3+} can be taken up within 30 min, indicating that this method has ultrahigh extraction efficiency. On the basis of the calculation, the extraction capacity of Tb^{3+} by nano-$Mg(OH)_2$ is as high as 1827 mg/g. It shows that $Mg(OH)_2$ plays not only the usual role of an adsorbent but also an ion-exchanger. In order to investigate the change in the ratio between Mg and Tb, the Mg and Tb contents in the solid phase as a function of time are listed in Table 1. Generally, the reaction rates of Mg and Tb can be expressed as: $r_{Mg} = -d[Mg]/dt$; $r_{Tb} = d[Tb]/dt$, respectively.

Table 1. Time Series of ICP Data of Extraction Experiment, the Mass Fraction of Tb and Mg in the Extractant, and the Concentration of Tb^{3+} and Mg^{2+} in Solution as a Function of Time

time (min)	Tb% in solid phase	Mg% in solid phase	C_{Tb3+} (mmol/L)	C_{Mg2+} (mmol/L)
0	0.00	41.4	40.0	0.00
1	7.66	34.8	30.1	14.9
3	27.2	21.4	13.8	39.3
5	35.8	14.7	8.60	47.1
7	41.6	9.81	5.43	51.9
10	46.1	8.50	4.38	53.4
15	48.1	5.76	2.96	55.6
20	50.7	5.00	2.47	56.3
25	52.4	3.98	1.93	57.1
30	54.4	3.62	1.70	57.5

After taking the derivative of the curve, $r_{Mg} = 2/3r_{Tb}$ is obtained. It indicates that 2 mmol Tb is extracted with the consumption of every 3 mmol $Mg(OH)_2$.

In order to examine the phase change during this process, as shown in Figure 2b, time-series XRD patterns were also obtained. In the first several minutes, two new peaks appeared at 10.3° and 28.4°. The extra peaks cannot be identified by the known compounds composed of Mg, Tb, O, and H from the PCPDF powder diffraction database. Since they do not belong to $Mg(OH)_2$, Tb-containing nanophase is assumed to have formed which corresponds to the ICP analysis. On the basis of the peak broadening using the Scherrer equation, the size of the nanoparticles (4–5 nm) remains unchanged as the reaction proceeds.

To verify the existence of nanoparticles and its micro-construction, the SEM and TEM images are given in Figure 3. The SEM images of the flowerlike nano-$Mg(OH)_2$ before, during, and after the extraction of Tb^{3+}, as shown in Figure 3a–c, respectively, indicate that the $Mg(OH)_2$ nanosheets were eroded and the surface became rough as the uptake process proceeded. In the images, it can also be seen that there may be the formation of small particles adhering to the magnesium hydroxide sheet. As shown in the inset of Figure 3c, many more grains exist on the surface of the nanoflower. It should be noted that the extractant still maintains its self-supported structure.

The HRTEM analysis of the sample at 30 min, as shown in Figure 3d, gives more information about the size and microstructure. Nanoparticles (4–5 nm) of uniform size can be observed on the nanosheets. The particle sizes depicted in the HRTEM images are consistent with the calculated values from the XRD patterns. Further analysis of the diffraction ring shows that the sample is polycrystalline, with the lattice spacing measured as d = 0.317 nm. This is identical to the calculated 28.4° from the XRD pattern by the Bragg equation. It demonstrates that these nanoparticles are the Tb compound with unknown chemical formula or structures.

Revealing the chemical structure of the unknown Tb compound is conducive to the study of the uptake mechanism. Pure-phase solid sample was obtained by reacting $Mg(OH)_2$ with an excess of Tb^{3+}. In Figure 4a showing the XRD pattern of the final product, two characteristic peaks at 10.3° and 28.4° of the Tb phase are consistent with Figure 2b. No diffraction peaks related to $Mg(OH)_2$ can be found, indicating this unknown compound is likely to be a pure nanophase. The valence state of the Tb nanocompound was determined by the XPS. Figure 4b shows the binding energy of Tb 4d orbital to be 146.47 eV, implying that Tb exists in a trivalent state after its

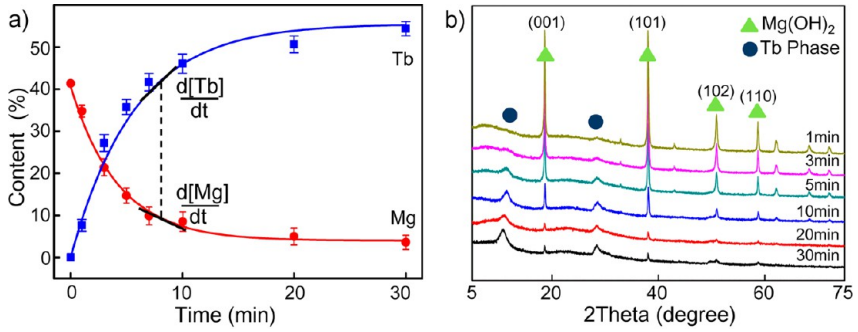

Figure 2. (a) The content of Mg and Tb in the solids at different reaction times. (b) Time series XRD analysis of precipitation solids from $Mg(OH)_2/Tb^{3+}$ reaction at room temperature.

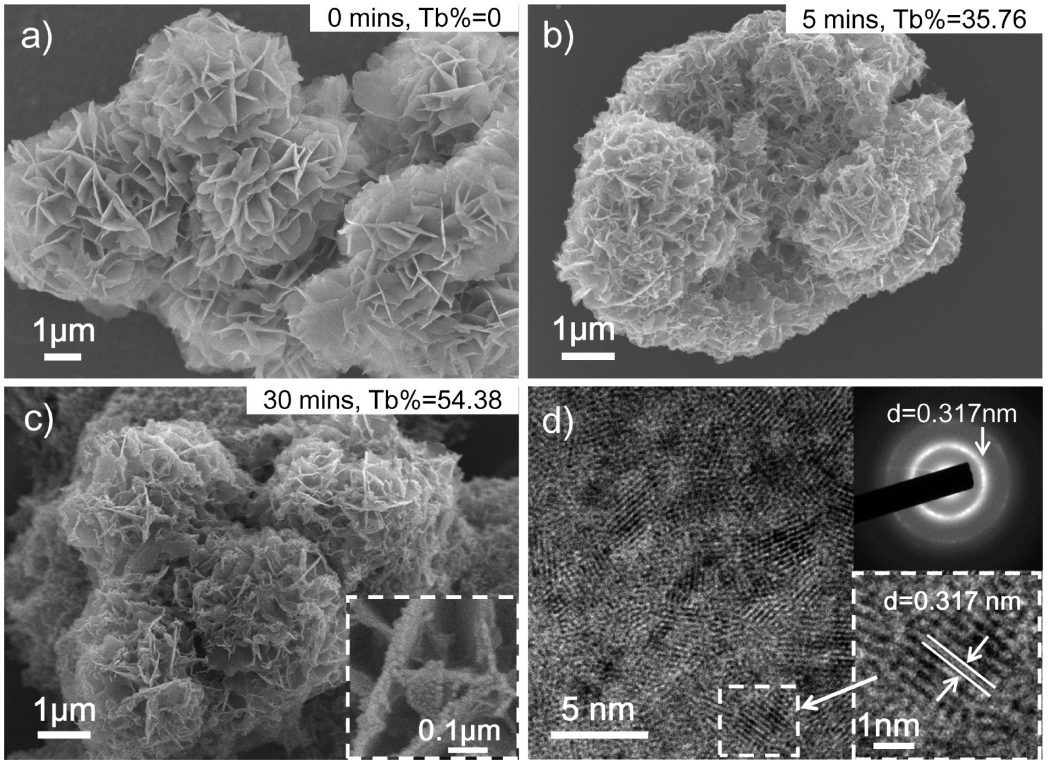

Figure 3. (a, b, and c) SEM images for the solid phase at time points of 0, 5, and 30 min. (d) HRTEM at 30 min (the insets are a diffraction image and the enlarged section of a single nanoparticle).

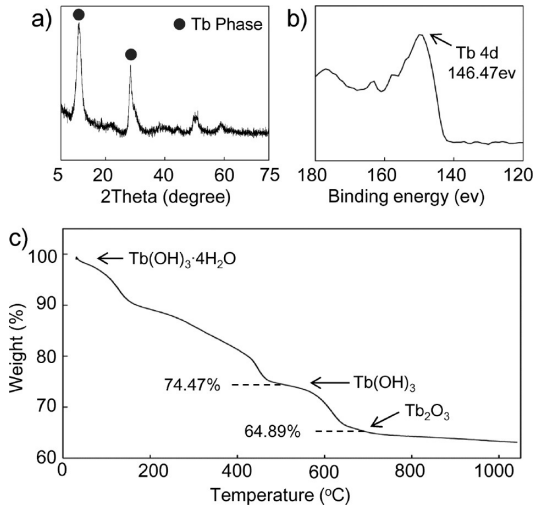

Figure 4. Analysis of the phase content of Tb: (a) XRD, (b) XPS, and (c) TGA data of Tb nanocompound under nitrogen protection. In the first stage, the weight loss of 25.53% with the loss of four crystal waters. In the second stage, there is a loss of 9.58% weight, possibly due to the dehydration of hydroxide transformed into the oxide.

transformation into nanomaterials.[27] The valence state is consistent with the curves calculated above (Figure 2a). The Tb formula weight of the compound, as calculated from Table 1, is about 280 g/mol. The EDS analysis of the Tb compound shows that it only contains oxygen, hydrogen, and Tb. On the basis of the valence state analysis and the formula weight, the product is inferred to be $Tb(OH)_3{\cdot}4H_2O$. Figure 4c shows the TGA curve, confirming the unknown Tb nanophase to be $Tb(OH)_3{\cdot}4H_2O$. The two-step dehydration is also in line with the general law of the thermal decomposition of hydrous compounds. The chemical structure is thus determined to be $Tb(OH)_3{\cdot}4H_2O$.

Uptake Mechanism. By analyzing the reaction product, the ion exchange reaction should be

$$Mg(OH)_2 + Tb^{3+} + 4H_2O \rightarrow Tb(OH)_3{\cdot}4H_2O + Mg^{2+} \quad (2)$$

As shown in Scheme 1, the reaction between nano-$Mg(OH)_2$ and REEs is speculated to be a cation exchange reaction from the magnesium hydrate nanosheet surface to internal layer by layer. First, there is an ionization balance between Mg^{2+} and the hydroxyl on the surface of $Mg(OH)_2$. Tb^{3+} bonds with the ionized hydroxyls to form terbium hydroxide depositing on the surface of nanosheet in situ. As hydroxides are consumed, magnesium hydroxide dissolves. In this case, following with the deposition of terbium hydroxide on the surface of the $Mg(OH)_2$ is leaching of Mg^{2+} into the solution. Once the deposited layer reaches a certain thickness, it hinders the dissolution of $Mg(OH)_2$. The ion exchange reaction ceased. As a result, a small portion of residual $Mg(OH)_2$ helps maintain the self-supported structure. In such an ion exchange process, the flowerlike nano-$Mg(OH)_2$ constructed by ultrathin lamellar structure could be helpful in REE recycling.

Uptake of Other REEs. The uptake of other REEs by nano-$Mg(OH)_2$ was evaluated in similar precipitation experiments. For four additional REEs on both sides of Tb in the periodic table, similar phenomena were observed. $Mg(OH)_2$ can immobilize other REEs besides Tb^{3+} by ion exchange (Figure 5). The XRD analysis suggests the generation of rare earth precipitates with the consumption of nano-$Mg(OH)_2$. On the basis of the peak at 30° in the XRD pattern, the products of different REEs should have different sizes. From light to heavy

dx.doi.org/10.1021/am4027967 | ACS Appl. Mater. Interfaces 2013, 5, 9719−9725

Scheme 1. Proposed Mechanism of Nano-$Mg(OH)_2$ Uptake of Tb^{3+} from Water[a]

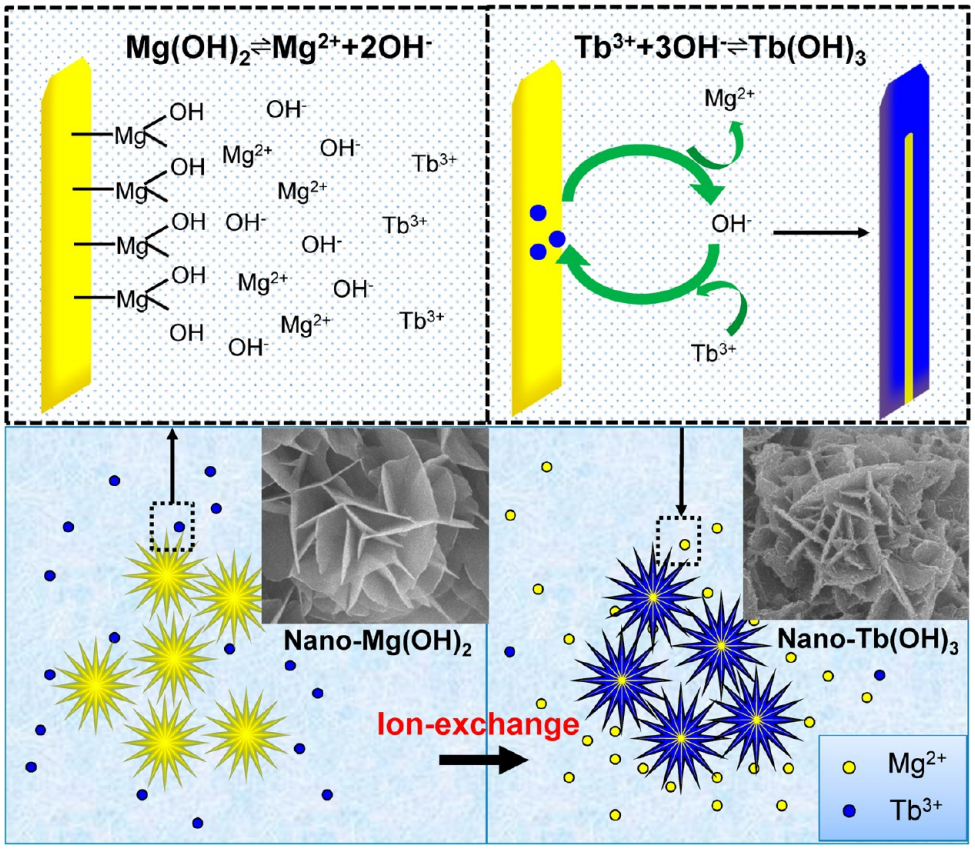

[a]First, there is an ionization balance between Mg^{2+} and the hydroxyl on the surface of $Mg(OH)_2$. Especially, concentration of radicals around the nanomaterials is likely to be much higher than that in the bulk. Thus, the concentrations of hydroxyl on the surface and around $Mg(OH)_2$ are relatively higher than those in solution. When Tb^{3+} comes close to the surface, with the K_{sp} of $Tb(OH)_3$ (2.0×10^{-22}) smaller than $Mg(OH)_2$ (1.8×10^{-11}), $Tb(OH)_3$ is more prone to precipitation. Tb^{3+} bonds with the ionized hydroxyl to form the terbium hydroxide precipitate, depositing on the surface of nanosheet in situ. As more and more hydroxides are consumed, magnesium hydroxide ionization equilibrium shifts to the right resulting in the leaching of Mg^{2+} to the solution.

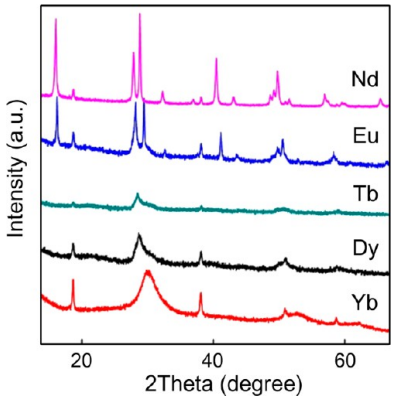

Figure 5. Series of XRD patterns of different rare earth metals (Nd, Eu, Tb, Dy, Yb) immobilized by magnesium hydroxide. $Mg(OH)_2$ (3 mmol) was suspended into 50 mL of REEs solution with an initial concentration of 0.04 mol/L.

rare earths elements, the size of the product evolves from bulk to nano and bulk mixture and then to the pure nanophase.

Column Extraction. Table 2 shows the concentration change of three Tb solutions (10.2, 94.3, 946 mg/L) before and after passing through a column (d = 3 cm) filled with 1.0 g of flowerlike nano-$Mg(OH)_2$ at a rate of 5 mL/min. The results

Table 2. Concentration Change of Tb^{3+} Solution before and after Passing through Nano-$Mg(OH)_2$ Reaction Column

initial concentration of Tb (mg/L)	equilibrium concentration of Tb (mg/L)
10.2	0.025
94.3	0.058
946	0.141

show a superb uptake effect for Tb at both low and high concentrations, with all the uptake rates higher than 99.7%.

Pilot-Scale Experiment. In the practical system, a bottleneck problem of the column method lies in how to achieve an effective uptake efficiency at a fast flow velocity. As an example of practical industrial wastewater, precipitate mother liquor[28] (30 L, pH = 7) was passed through a column packed with 10.0 g of self-supported flowerlike nano-$Mg(OH)_2$ and a column packed with 10.0 g (Figure 6a). As shown in Figure 6b, the flow rate of the commercial $Mg(OH)_2$ column decreased rapidly, while the flow rate of the flowerlike $Mg(OH)_2$ column basically remained unchanged within 60 min. Under this high flow rate condition, the percentage of REEs uptake is shown in Figure 6c. More than 85% REEs can be immobilized. After going through two continuous columns, the uptake rate could reach 99%. The self-supported structure guarantees both high flow rate and efficiency in the practical process.

dx.doi.org/10.1021/am4027967 | ACS Appl. Mater. Interfaces 2013, 5, 9719−9725

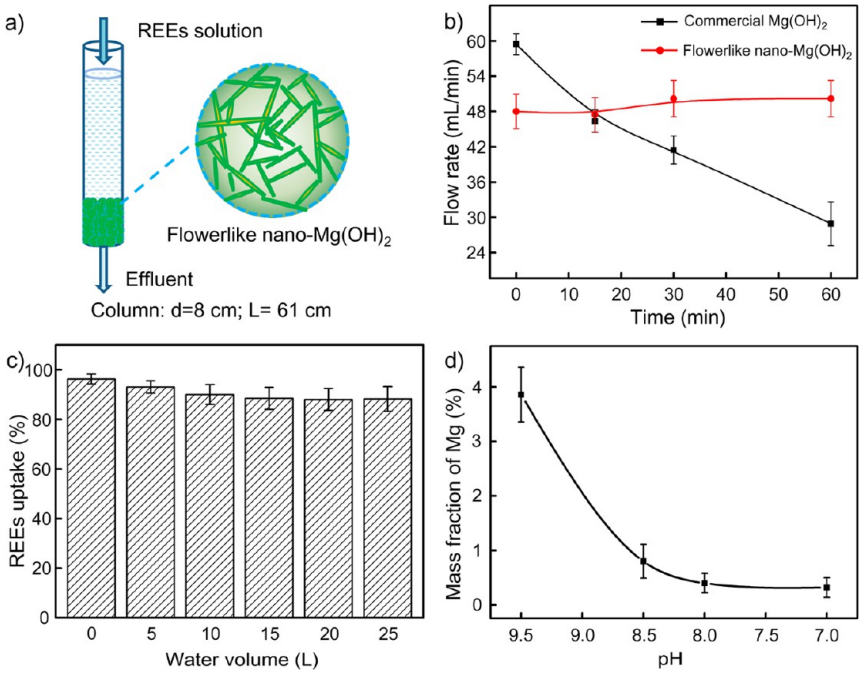

Figure 6. (a) Schematic illustration of the column operations. The column (d = 8 cm) was filled with 10.0 g of nano-$Mg(OH)_2$ (apparent density is 0.238 g/cm^3); REEs solution (30 L) flushed through the column (the aspect ratio = L/d = 7.6). (b) The flow rate of commercial $Mg(OH)_2$ and flowerlike nano-$Mg(OH)_2$ changed with time. (c) The percentage of REEs uptake by passing through the column filled with flowerlike nano-$Mg(OH)_2$. (d) The mass fraction of the residual Mg changes as a function of pH.

The solid phase after the column extraction contained a part of the residual magnesium hydroxide in addition to a large quantity of rare earth hydroxides. To obtain pure rare earth products, the solid in the column was transferred to a small amount of aqueous solution, after adjusting the pH to 7 with 1.0 M HCl. In Figure 6d, the mass fraction of the residual Mg decreases from 3.86% to 0.32% as pH changes from 9.5 to 7.0. Meanwhile, the rare earth still exists in the solid phase and hardly dissolves into the solution because of a low K_{sp} value of 2.0×10^{-22}. Pure rare earth products can then be obtained after centrifugation and calcination. According to calculations of the uptake rate and the water yield, nearly 100 kg of REEs could be extracted from such wastewater each day.

4. CONCLUSION

In summary, self-supported flowerlike nano-$Mg(OH)_2$ was produced by a low-cost magnesium salt chemical precipitation method. It showed superb properties to uptake REEs from wastewater. In a practical test, the extractant exhibited both high flow rate and high efficiency with a maximum capacity of 1827 mg/g. An ion-exchange mechanism between magnesium ion and rare earth ion was proposed. Because of the ultrahigh extraction efficiency, low-cost $Mg(OH)_2$ gets high value-added nano-rare earth in return. Recycling REEs from wastewater not only saves rare earth resources and protects the environment but also brings considerable economic benefits. The pilot-scale experiment indicated that the self-supported flowerlike nano-$Mg(OH)_2$ had great potential to recycle REEs from industrial wastewater.

AUTHOR INFORMATION

Corresponding Author

*E-mail: zlin@fjirsm.ac.cn. Tel/Fax: (+086)591-83705474.

Notes

The authors declare no competing financial interest.

ACKNOWLEDGMENTS

Financial support was provided by the National Basic Research Program of China (2010CB933501, 2013CB934302), the Outstanding Youth Fund (21125730), the National Natural Science Foundation of China (21273237, 21103191), Fund of Fujian Key Laboratory of Nanomaterials (2006L2005), the Fujian Science Foundation Grant (2012J05035) and the Knowledge Innovation Program of the Chinese Academy of Sciences (KJCX2-YW-N50, KJCX2-EW-J02).

REFERENCES

(1) Sorace, L.; Benelli, C.; Gatteschi, D. *Chem. Soc. Rev.* **2011**, *40*, 3092−3104.
(2) Binnemans, K. *Chem. Rev.* **2009**, *109*, 4283−4374.
(3) Trovarelli, A. *Catal. Rev.* **1996**, *38*, 439−520.
(4) Bogdanović, B.; Felderhoff, M.; Pommerin, A.; Schüth, F.; Spielkamp, N. *Adv. Mater.* **2006**, *18*, 1198−1201.
(5) de la Cruz, C.; Huang, Q.; Lynn, J. W.; Li, J.; Ratcliff, W., 2nd; Zarestky, J. L.; Mook, H. A.; Chen, G. F.; Luo, J. L.; Wang, N. L.; Dai, P. *Nature* **2008**, *453*, 899−902.
(6) Chen, Z. *J. Rare Earth* **2011**, *29*, 1−6.
(7) Itoh, M.; Miura, K.; Machida, K.-i. *J. Alloys Compd.* **2009**, *477*, 484−487.
(8) Kim, J. Y.; Kim, U. S.; Byeon, M. S.; Kang, W. K.; Hwang, K. T.; Cho, W. S. *J. Rare Earth* **2011**, *29*, 1075−1078.
(9) Yang, H.; Wang, W.; Cui, H.; Zhang, D.; Liu, Y.; Chen, J. *J. Chem. Technol. Biotechnol.* **2012**, *87*, 198−205.
(10) Pietrelli, L.; Bellomo, B.; Fontana, D.; Montereali, M. R. *Hydrometallurgy* **2002**, *66*, 135−139.
(11) Jun, T.; Jingqun, Y.; Kaihong, C.; Guohua, R.; Mintao, J.; Ruan, C. *Int. J. Miner. Process.* **2011**, *98*, 125−131.
(12) Chi, R.; Xu, Z. *Metall. Mater. Trans. B* **1999**, *30*, 189−195.

(13) Chi, R.; Hu, Y.; Zhu, G.; Xu, S.; Zhou, Z.; Xu, Z. *Metall. Mater. Trans. B* **2003**, *34*, 611−617.
(14) Coppin, F.; Berger, G.; Bauer, A.; Castet, S.; Loubet, M. *Chem. Geol.* **2002**, *182*, 57−68.
(15) Babel, S.; Kurniawan, T. A. *J. Hazard. Mater.* **2003**, *97*, 219−243.
(16) Cao, Q.; Huang, F.; Zhuang, Z.; Lin, Z. *Nanoscale* **2012**, *4*, 2423.
(17) Mohmood, I.; Lopes, C. B.; Lopes, I.; Ahmad, I.; Duarte, A. C.; Pereira, E. *Environ. Sci. Pollut. Res.* **2013**, *20*, 1239−1260.
(18) Fu, F.; Wang, Q. *J. Environ. Manage.* **2011**, *92*, 407−418.
(19) Warner, C. L.; Addleman, R. S.; Cinson, A. D.; Droubay, T. C.; Engelhard, M. H.; Nash, M. A.; Yantasee, W.; Warner, M. G. *ChemSusChem* **2010**, *3*, 749−757.
(20) Tan, X. L.; Fan, Q. H.; Wang, X. K.; Grambow, B. *Environ. Sci. Technol.* **2009**, *43*, 3115−3121.
(21) Liu, W.; Huang, F.; Wang, Y.; Zou, T.; Zheng, J.; Lin, Z. *Environ. Sci. Technol.* **2011**, *45* (5), 1955−1961.
(22) Li, B. J.; Cao, H. Q.; Yin, G. *J. Mater. Chem.* **2011**, *21*, 13765−13768.
(23) Zhang, S.; Cheng, F. Y.; Tao, Z. L.; Gao, F.; Chen, J. *J. Alloys Compd.* **2006**, *426*, 281−285.
(24) Cao, C. Y.; Qu, J.; Wei, F.; Liu, H.; Song, W. G. *ACS Appl. Mater. Interfaces* **2012**, *4*, 4283−4287.
(25) Wang, Y.; Chen, D.; Wang, Y.; Huang, F.; Hu, Q.; Lin, Z. *Nanoscale* **2012**, *4* (12), 3665−3668.
(26) Zhang, S.; Li, J.; Wen, T.; Xu, J.; Wang, X. *RSC Adv.* **2013**, *3*, 2754.
(27) Moulder, J. F.; Stickle, W. F.; Sobol, P. E.; Bomben, K. D. *Handbook of X-ray Photoelectron Spectroscopy*; Physical Electronics Division, Perkin-Elmer Corp.: Eden Prairie, MN, 1992.
(28) In the rare earth separation and purification process, mother liquor is one type of wastewater whose concentration of REE is relatively high (127.42 mg/L). Water yield is 766.54 tons of wastewater containing only a single REE generated each day in a factory. The ICP test of this wastewater shows the concentration of other elements, i.e., Ca 2.34 mg/L, Fe 0.19 mg/L, Cu 0.012 mg/L, Zn 2.37 mg/L, Mn 0.006 mg/L, and Cr 0.007 mg/L, with K, Na, and Pb not detected.